Received: 26 March 2020 | Revised: 12 January 2021 | Accepted: 11 February 2021

IET Microwaves, Antennas & Propagation

DOI: 10.1049/mia2.12111

The Institution of Engineering and Technology WILEY

ORIGINAL RESEARCH PAPER

Wideband circularly polarised antenna array with isoflux pattern

Fanchao Zeng[1] | Zhi-Ya Zhang[1,2] | Yang Feng[1] | Shaoli Zuo[3] | Chengbin Zhang[1] | Li Wang[1]

[1]National Key Laboratory of Antennas and Microwave Technology, Xidian University, Shaanxi, China

[2]Collaborative Innovation Center of Information Sensing and Understanding at Xidian University, Shaanxi, China

[3]School of Physics and Optoelectronic Engineering, Xidian University, Xi'an, Shaanxi, China

Correspondence

Zhi-Ya Zhang, Collaborative Innovation Center of Information Sensing and Understanding at Xidian University, Shaanxi, China.
Email: zhiyazhang@163.com

Funding information

The Fundamental Research Funds for National Natural Science Foundation of China, Grant/Award Number: 61601338; The Fundamental Research Funds for National Natural Science Foundation of China, Grant/Award Number: 61671349; Fundamental Research Funds for Central Universities of the Central South University, Grant/Award Number: JB180207

Abstract

The authors present a wideband circularly polarised antenna array consisting of a 10-element ellipse dipole antenna and a feed network. A metal pillar is vertically loaded at the end of each ellipse dipole arm to extend the current path, thereby reducing the lateral dimension of the antenna element. For uniform coverage over the Earth's surface, antenna with an isoflux pattern is required due to its uniform power density over a wide coverage area. To obtain wideband and isoflux characteristics, the amplitude and phase distributions along the network are optimised by applying the hybrid of the genetic algorithm and particle swarm optimisation. Particularly, the feed network with broadband phase shifting performance is designed to attain a broad bandwidth requirement. The proposed antenna can achieve excellent impedance matching and axial ratio characteristics from 1.1 to 1.6 GHz. In addition, the isoflux radiation pattern is obtained with the beamwidth of ±21° where the gain is higher than 0 dBi in the elevation plane (xoz-Plane). The realised gain is better than 10.2 dBi and the side lobes are below −14.2dB across the operating frequency. Finally, the antenna array is manufactured and measured, and good agreement is achieved between the simulation and measurement results.

1 | INTRODUCTION

Circularly polarised (CP) antenna are widely used in global navigation satellite system (GNSSs), satellite communication systems, radio frequency identification, and wireless power transmission systems due to their capabilities of reducing polarisation mismatch and suppressing multipath interferences [1–4]. These CP antennas are developed by using different approaches [1], such as excitation of two degenerate resonant modes and sequential arrangement of four linearly polarised antenna elements with 90° phase delay. For expanding the CP bandwidth, external feed networks comprising of the Wilkinson power divider (PD) and the 90° phase shifter (PS) have been employed to increase the bandwidth of the dual-feed CP antennas [5–7]. Patch antennas [8–12] also can achieve broad CP bandwidth. However, the size of patch antenna is normally quite large.

Isoflux radiation pattern [13–17] has a wide range of applications in wireless communications. In [13], an isoflux pattern antenna operating in the X-band which was used in transmitting the specific absorption rate data from the low Earth orbit (LEO) satellite was presented. By employing a ridged aperture and multistage choke rings, the desired shaped pattern was achieved. The design in [15] developed a modified S-band satellite antenna using two crossed dipole elements and a PD as the feeding network, but it exhibited a relatively narrow input fractional impedance bandwidth of approximately 4.8%. A planar metasurface isoflux-type antenna was designed and manufactured for the LEO satellite application in [14], which was excited by a surface wave generated by a coplanar feeder. However, the impedance bandwidth is only 2.3%. In [18], a compact X-band antenna, consisting of a driving patch antenna and 12 parasitic crossed dipoles, achieved an isoflux shaped beam with

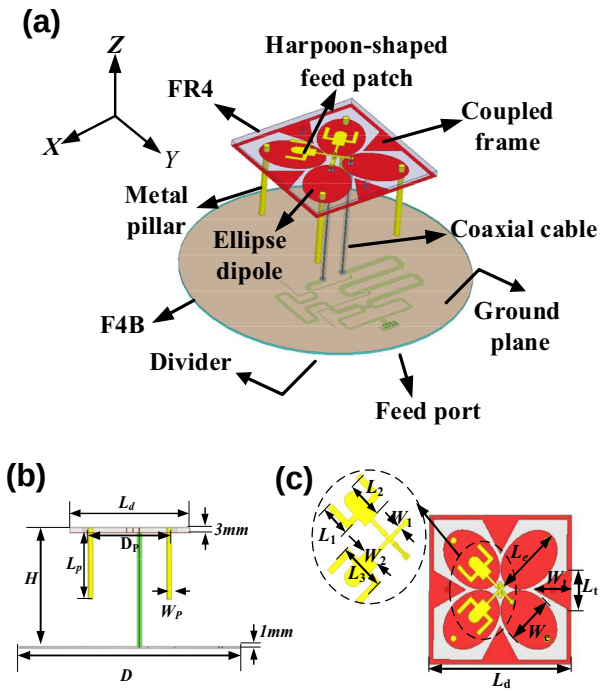

FIGURE 1 Configuration of the antenna element: (a) perspective view, (b) side view, and (c) top view

circular polarisation. Regretfully, the exact isoflux radiation objective could not be achieved due to the platform size.

Here, a wideband CP antenna array with isoflux shaped pattern is presented, which adopts a corporate-fed network [19] to provide the required amplitude and phase distribution. By introducing the harpoon-shaped feed patch and a square coupling frame, the impedance bandwidth of the element is effectively improved from 0.96 to 1.7 GHz, without using any impedance matching circuits. More than that, the open and short lines are employed to smooth the phase variation in the feed network. The measured results of the array antenna indicate that the frequency bandwidth for voltage standing wave ratio (VSWR)≤1.5 and axial-ratio (AR)≤3 dB ranges from 1.1 to 1.6 GHz. Particularly, conical-like isoflux pattern characteristics are obtained at a cone of ±21° where a gain of more than 0 dBi in the elevation plane was observed. The side lobes are below −14.2 dB, and the gain of the antenna is better than 10.2 dBi over the entire operating band.

2 | ANTENNA DESIGN AND DISCUSSION

2.1 | Design of the element

The geometry of the proposed CP antenna element is illustrated in Figure 1(a), (b), and (c). From Figure 1(a) and (b), it is noted that a pair of elliptical printed dipoles are placed orthogonally on the lower side of the FR4 substrate, which has a relative dielectric constant of $\varepsilon_r = 4.4$, a loss tangent of 0.02, and a thickness of 3 mm. In order to increase the gain and impedance bandwidth of the antenna, a square coupling frame is employed around the crossed dipole antenna. Moreover, a metal pillar with length L_p is employed at the end of each ellipse dipole arm to extend the current path, thereby reducing the lateral dimension of the dipole element. The overall size of the antenna is $0.31\lambda_0 \times 0.31\lambda_0 \times 0.27\lambda_0$ (λ_0 is the free-space wavelength at 1.35 GHz). The upper side of the dielectric substrate is printed with two orthogonal harpoon-shaped feed patches as shown in Figure 1(c). To avoid electrical contact, one of harpoon-shaped feed lines is modified. One part of the line is printed on the bottom face of the substrate, and then is connected to the top parts with two shorting pins. For the feed network as shown in Figure 1(a), the crossed dipole elements are fed by the Wilkinson PD (on the lower surface of F4B) with 90° PS. This PS is essential for generating the CP radiation. In this design, a pair of open and short lines with a length of $\lambda_g/8$ is employed to get a flat phase variation over the whole bandwidth, where λ_g is the wavelength on the substrate at the centre frequency of 1.35 GHz. The final optimal antenna parameters are shown in Table 1.

TABLE 1 Dimensions of the proposed antenna (mm)

Parameter	Value	Parameter	Value
L_d	70	D	130
D_p	45	W_d	85
L_p	36	W_t	17.7
W_p	3	L_t	18
H	60	W_e	22.8
L_1	10	L_e	32
L_2	11.8	W_2	6
W_1	1.2		

2.2 | Optimisation and pattern synthesis

2.2.1 | Construction of the objective function

In the design of antenna element, the metal pillar serves to extend the current path. The relationship between performance of antenna element and the metal pillar is depicted in Figure 2. Obviously, with the gradual increase of *h1*, the resonant frequency of the antenna moves to the low frequency. At the same time, the gain of low frequency first increases and then decreases, while the gain of high frequency shows a decreasing trend, as shown in Figure 2(a) and (c).

Figure 2(b) and (d) shows the change curve of VSWR and antenna gain with frequency and T. when $T = 2$, 3, and 4 mm (the diameter of the short-circuit column increases from 2 to

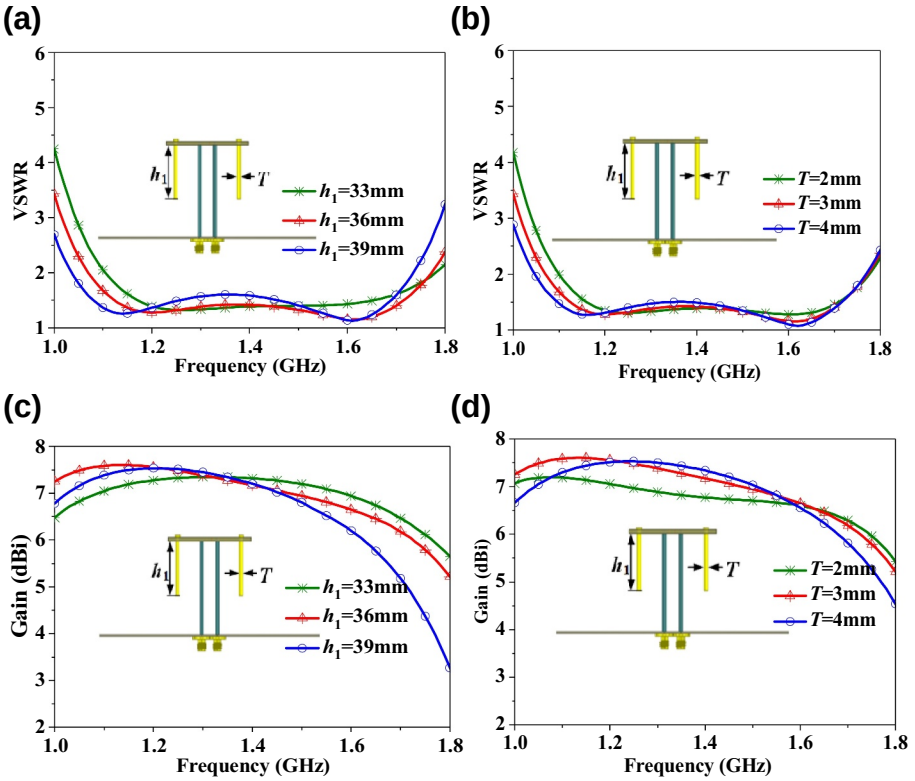

FIGURE 2 Performance changes of the antenna element by the metal pillar. (a) changes of VSWR with different h1, (b) changes of VSWR with different T, (c) changes of gain with different h1, and (d) changes of gain with different T. VSWR, voltage standing wave ratio

4 mm), the impedance bandwidth of the antenna becomes wider. Because the characteristic impedance is reduced by the thicker metal column, the input impedance curve becomes flatter. Besides, the gain of the intermediate frequency decreases as T increases, and the low and high frequency gains decrease as T increases.

The Figure 3(a) and (b) show that the element has a fractional impedance bandwidth of 55.6% for VSWR≤1.5 ranging from 0.96 to 1.7 GHz and a 3-dB AR bandwidth of 56.1% ranging from 1.0 to 1.78 GHz. Due to the loading effect of square coupling frame, the element can achieve a relative higher gain. The simulated antenna gain varies from 6.25 to 6.55 dBi over the whole band. Moreover, the radiation efficiency of the antenna in the operating frequency band is higher than 78%.

The *xoz*-plane and *yoz*-plane radiation at 1.145, 1.279 and 1.591 GHz are plotted in Figure 4(a)(c). At each frequency, the half-power beamwidth of the core polarisation patterns are 82, 86 and 90°, respectively. For the entire half-power beamwidth, the AR is below 3-dB. The simulation results (Figure 3) show that the broadband antenna element has a good impedance match and CP radiation characteristics, which is a good candidate as an element of the broadband CP antenna array.

To provide a uniform power density on ground, the antenna mounted on the satellite must compensate the power loss due to the propagation path by increasing the gain towards

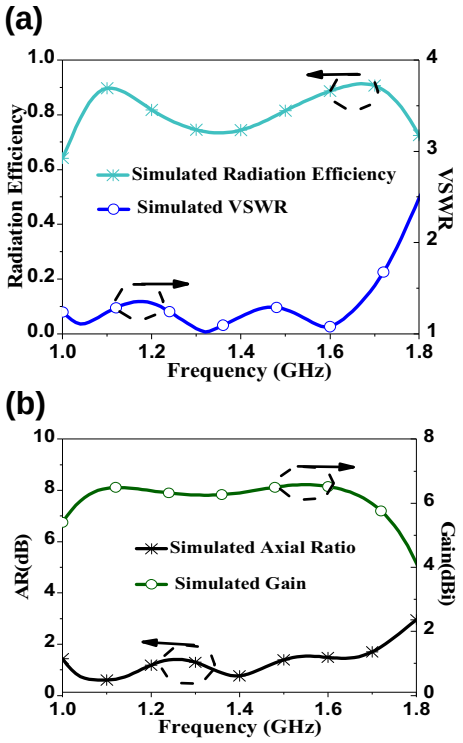

FIGURE 3 The simulated results of (a) efficiency and VSWR, and (b) gain and AR against frequency. VSWR, voltage standing wave ratio

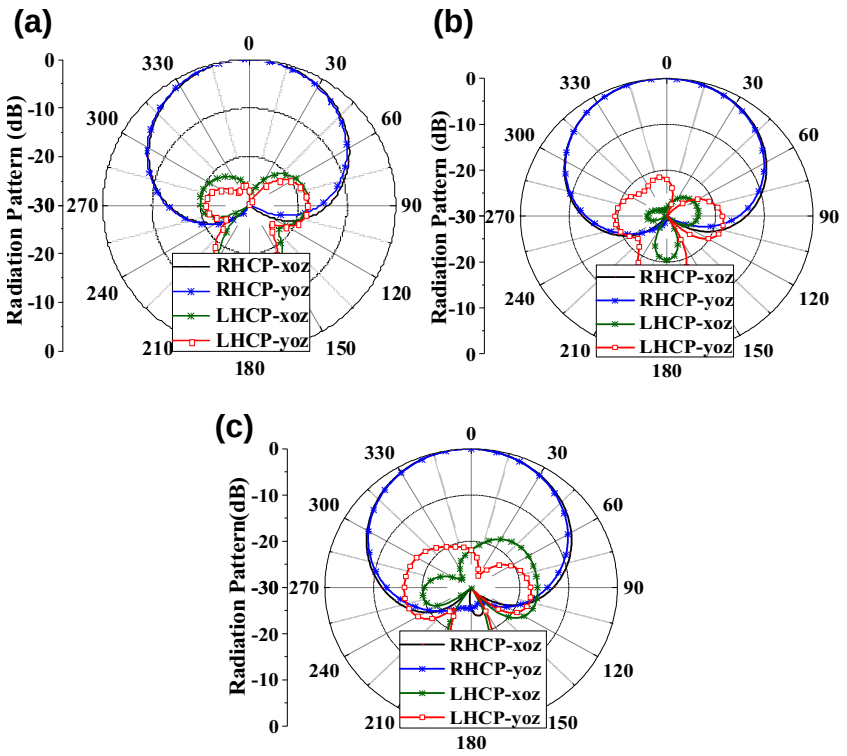

FIGURE 4 Simulated radiation patterns at (a) 1.145 GHz, (b) 1.279 GHz, and (c) 1.591 GHz in the xoz-plane and yoz-plane

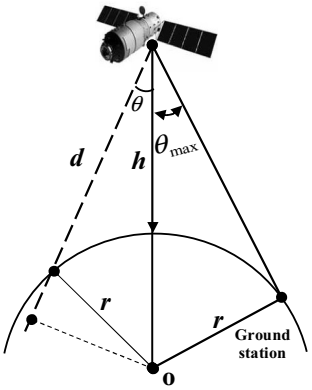

FIGURE 5 Sketch of the Earth-satellite geometry

directions where the path is longer. Figure 5 shows a sketch of the Earth-satellite geometry. There, r is the radius of the Earth, h is minimum distance from the satellite to the Earth surface, $\theta_{\max}$ is the maximum coverage angle, and d is the distance of the satellite from any point at the coverage area on the ground Figure 6.

The distance from the satellite to the surface of the Earth is given by its orbit, so h is known. Then, $d_{\max}$ is calculated using the Pythagorean theorem and $\theta_{\max}$ is obtained which is as follows:

$$\sin\theta_{\max} = r/(r+h) \tag{1}$$

d is calculated as follows:

$$d = (r+h)\left(\cos\theta - \sqrt{\sin^2\theta_{\max} - \sin^2\theta}\right) \tag{2}$$

where $d \in [h,(r+h)^2 - r^2]$.

Radiation pattern function $f_{aim}(\theta)$ can be describe as follows:

$$f_{aim}(\theta) = \frac{U(\theta)}{C}(r+h)\left(\cos\theta - \sqrt{\sin^2\theta_m - \sin^2\theta}\right) \tag{3}$$

where $U(\theta)$ is radiant energy intensity and C is a constant.

Then, the normalised objective function is obtained as:

$$f_{aim}(\theta) = \begin{cases} A \Big/ \cos\left(\dfrac{\sin(\theta)}{\sin(\theta_m)} \cdot \arccos A\right) & |\theta| \in [0, \theta_m] \\ B/\sin^5\theta & |\theta| \in (\theta_m, \theta_1] \end{cases} \tag{4}$$

where θ_m corresponds to the angle of the peak gain and θ_1 corresponds to the angle of the sidelobe level.

Adjusting the value of A can change the magnitude of the concave. In this design, A is designed as 0.8, B is calculated to be 0.0074 according to [14] and the criteria $\theta \in (0,\theta_{\max})$.

2.2.2 | Construction of fitness function

In order to obtain an isoflux radiation pattern, the amplitude and phase distribution along the feed are optimised by applying

FIGURE 6 The proposed antenna array

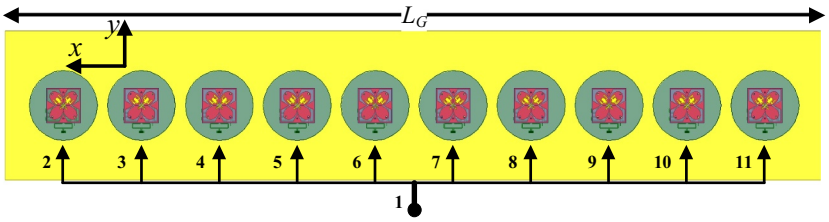

TABLE 2 Optimised values of amplitude and phase distribution

Excitations			
Port	**Amplitude**	**Power**	**Phase (degrees)**
2	0.591	0.35	−246
3	0.775	0.6	−141
4	0.927	0.86	−116
5	0.837	0.7	−61
6	1.0	1.0	0
7	1.0	1.0	0
8	0.837	0.7	−61
9	0.927	0.86	−116
10	0.775	0.6	−141
11	0.591	0.35	−246

the hybrid of the genetic algorithm (GA) and particle swarm optimisation (PSO) methods. Figure 6 shows a linear array that is deployed along the x-axis, which consists of 10 crossed dipole elements.

The far-field radiation pattern of array can be described as follows:

$$E(\lambda,\theta)=\sum_{n=1}^{N}\alpha\exp\left(j\left(\frac{2\pi}{\lambda}(n-1)d\cdot\cos\theta+\beta\right)\right)\cdot g(\theta) \tag{5}$$

where θ is the angle between the axis of the array (x-axis) and the radial vector from the origin to the observation point, λ is the wavelength, d is the distance between the adjacent elements, α and β are the amplitude and phase excitation coefficients, respectively. $g(\theta)$ is the element radiation pattern, which embodies the influence of mutually coupled array, edge effect and ground plane.

Suppose that the desired radiation pattern of the linear antenna array is $E_d(\lambda_i,\theta)$, and its actual radiation pattern function is $E_a(\lambda_i,\theta)$. Thus the deviation between the desired pattern and the actual one is

$$m_e=E_a(\lambda_i,\theta_m)-E_d(\lambda_i,\theta_m)m=1,\ 2,\ \ldots,M \tag{6}$$

where M represents the number of sampling points in main beam.

Least mean square error of main beam is obtained as follows:

$$M_u=\left(\frac{1}{N}\sum_{n=1}^{N}|m_e|^2\right)^{\frac{1}{2}} \tag{7}$$

Similarly, the deviation between the expected side lobe ($PSLL_{aim}$) and the actual one ($PSLL_1$) is:

$$M_p=PSLL_1-PSLL_{aim} \tag{8}$$

The fitness function is defined as follows:

$$Fit=\eta_1\cdot M_U+\eta_2\cdot M_P \tag{9}$$

where η_1 and η_2 represent the weight of M_u and M_p, respectively. It is worth noting that actualvalues may be less than the desired one. Therefore, there is section statement within the algorithm to avoid this situation. If $PSLL_1 \le PSLL_{aim}$, η_2 is equal to zero.

Considering that the array is symmetric with respect to x-axis, the symmetrical amplitude and phase distributions of element are applied to reduce the number of optimised variables. For consideration of the feed network manufacturability, the amplitude and phase distributions of element are limited in [0.3, 1] and [0, 360], respectively. The algorithmic parameter values in the optimisation are: $\eta_1 = 0.65$ and $\eta_2 = 0.35$, respectively.

The 10-element linear array is optimised to produce an isoflux beam pattern with a −14.0 dB side lobe level (SLL). Table 2 shows the amplitude and phase distributions of the feed.

The optimum radiation patterns obtained using the hybrid of GA and PSO methods and from simulation in the commercial EM-simulator HFSS 13.0 are shown in Figure 7(a), (b), and (c). It is noted that, the first SLL and isoflux beam pattern level obtained by the hybrid of GA and PSO are very similar to the simulated results. Furthermore, the radiation pattern is almost identical to our targeted isoflux pattern, and the maximum SLL for the co-pol pattern of the array is less than −15.4dB in the elevation plane. Particularly, the isoflux beamwidth angle range is obtained at a cone of ±2° where the gain is higher than 0 dBi in elevation plane. In the azimuth-plane (yoz-Plane), the co-pol patterns have a 3-dB

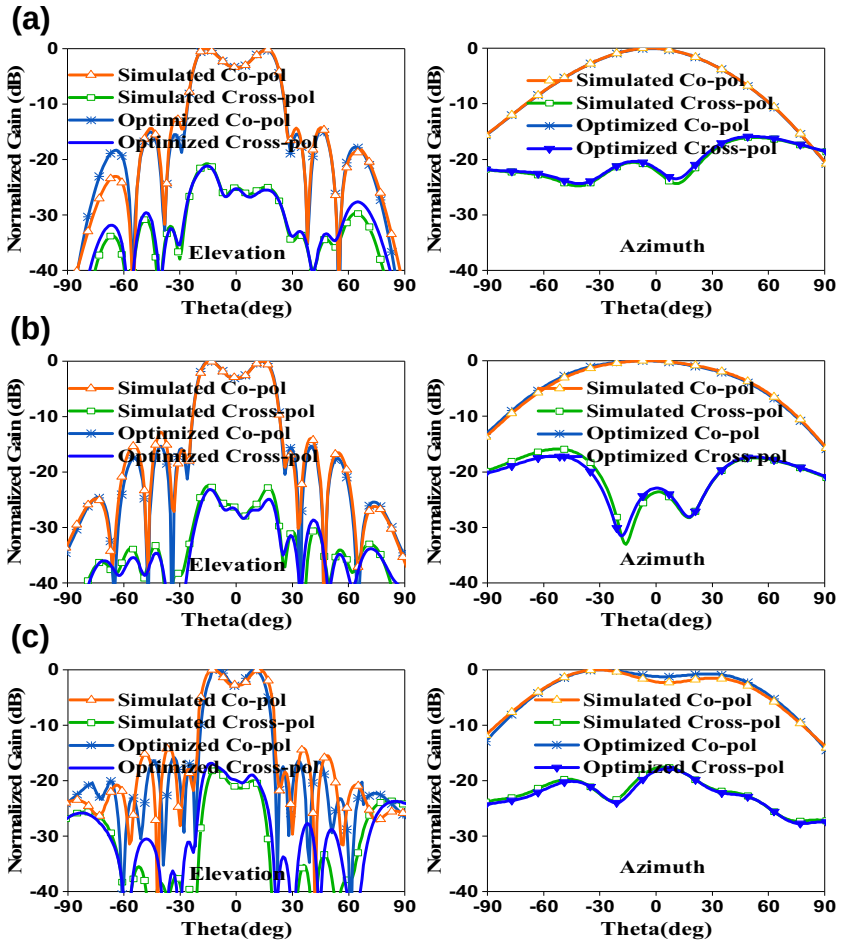

FIGURE 7 Optimiszed radiation patterns with the hybrid of GA and PSO and simulated with the EM-simulator HFSS 13.0 at (a) 1.145 GHz, (b) 1.279 GHz, and (c) 1.591 GHz

beamwidth of approximately 69°. The cross-polarisation levels are −16.1, 16.5, and 16.3 dB at 1.145, 1.279, and 1.591 GHz, respectively. There is reasonable agreement between the simulated and optimised radiation patterns.

2.3 | Feed network of the 10-element linear array

Considering that the feed network is symmetrical, the symmetrical amplitude and phase distribution of element are achieved. Figure 8 reveals the measured S-parameters from 1.1 to 1.6 GHz and the phase of each output port is normalised to port 6. The return losses are lower than −12 dB. The isolation between the output ports is better than 15.0 dB over the entire operating band. Particularly, the open and short lines are deployed to smooth the phase variation, thus the feed network exhibits broadband phase performance.

In order to verify the isoflux radiation characteristics, a coplanar feed network is designed using the commercial EM-simulator HFSS13.0 and manufactured on a polytetrafluoro-ethylene substrate which has a relative permittivity of 2.65, a loss tangent of 0.002, and a thickness of 1 mm. In Figure 9(a), the coplanar feed network formed of nine Wilkinson PDs and PSs is designed to provide high isolation and desired power ratio. Particularly, a broadband PS is employed to get a flat phase characteristic in the operating band. The fabricated wideband feed network is shown in Figure 9(b).

The details of the measured and simulated S-parameters are shown in Table 3. The phase differences between measured and simulated results are within ±4.5°. However, the transmission coefficients of the simulation are smaller than the theoretical value due to the dielectric and reflection loss. Specifically, the measured magnitude of S-parameters is around 0.1 to 0.4 dB less than the simulated result, which is very similar to the theoretical values. All of the above results show that the feed network achieves desired wideband characteristic and power distribution performance.

3 | MEASUREMENT RESULTS

The developed 110 antenna array was fabricated and the photograph of the prototype is shown in Figure 10. The linear array consists of 10 elements, a feed network, and a metal plane. The crossed dipole elements are placed on the front side of the metal plate, and the microstrip feed lines, numbered sequentially per the corresponding radiators, are shown on the bottom side. Its element spacing is 158 mm ($0.71\lambda_0$). The

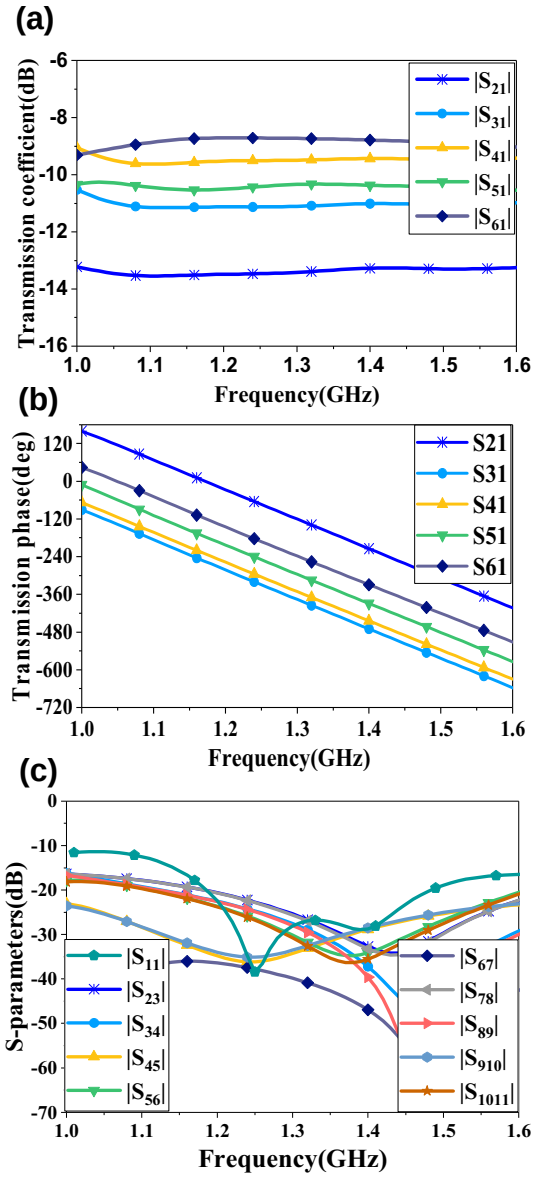

FIGURE 8 S-pardummeters parameters of the feed network: (a) Transmission transmission coefficient (b) Transmission transmission phase and (c) S-parameters

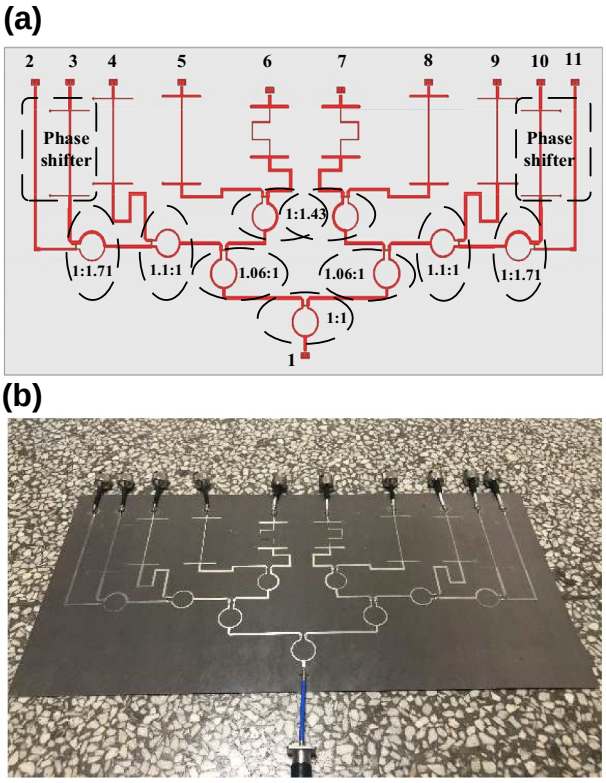

FIGURE 9 Wideband feed network. (a) layout diagram and (b) prototype photograph

length and width of the ground plane are, $L_G = 1700$ mm and $W_G = 300$ mm, respectively.

The measured results were obtained using an Agilent E8363 B network analyser and an anechoic chamber. Figure 11 (a) and (b) shows the measured results of the antenna array, and it can be seen that the proposed antenna achieves a measured impedance (VSWR≤1.5) and AR≤3 bandwidth ranging from 1.1 to 1.6 GHz. Meanwhile, the gain of the array combined with the feed network is better than 10.2 dBi over the operating band.

Meanwhile, the measured and simulated radiation patterns of the antenna array in both elevation and azimuth planes at 1.145, 1.279, and 1.591 GHz, are shown in Figure 12(a)–(c), respectively. The maximum SLL is below −14.2 dB in the elevation plane. The maximum radiation occurs at the main beam direction of $\theta = 14$–$16°$ while the gain reaches 10.6 dBi at 1.145 GHz. As the frequency increases, the conical radiation pattern is narrowed by about 4°, and the gain variation for the co-polarisation is less than 1.5 dB. Meanwhile, the gain at $\theta = 0°$ are about 3 dB less than the peak gain, which is similar to the simulated results. In the azimuth plane, the co-polarisation patterns have a 3-dB beamwidth of approximately 67°. Moreover, the measured crossed-polarisation level is lower than −15.6 dB. Finally, an acceptable agreement between the simulated and measured results validates the proposed antenna. To further illustrate our design, a comparison table with other works is listed in Table 4.

4 | CONCLUSION

A wideband CP antenna array with the isoflux radiation pattern has been successfully designed and manufactured for the satellite application. First, the element has a fractional impedance bandwidth of 55.6% for VSWR≤1.5 ranging from 0.96 to 1.7 GHz and a 3-dB AR bandwidth of 56.1% ranging from 1.0 to 1.78 GHz and the antenna array has achieved a good impedance matching and wideband AR characteristic from 1.1 to 1.6 GHz. Furthermore, the particular radiation pattern exploited in the design is achieved by applying the hybrid of GA and PSO optimisation methods. To verify the isoflux radiation characteristics, a coplanar feed network is designed and manufactured. Finally, the isoflusx angle is obtained at a cone of ±21° where the gain is more than 0 dBi in the elevation plane.

TABLE 3 Amplitude and phase distribution of the feed work

Theoretical Value		Simulated value			Measured value		
Frequency (GHz)		1.145	1.279	1.591	1.145	1.279	1.591
|S12| (dB)	−13.0	−13.5	−13.4	−13.3	−13.8	−13.5	−13.4
Phase (°)	−246	−242	−242	−251	−244	−243	−247
|S13| (dB)	−10.1	−11.1	−11.1	−11.0	−10.9	−10.8	−10.6
Phase (°)	−141	−136	−137	−145	−140	−141	−143
|S14|(dB)	−9.1	−9.6	−9.5	−9.4	−9.8	−9.6	−9.6
Phase (°)	−116	−112	−112	−118	−115	−116	−119
|S15|(dB)	−10.0	−10.5	−10.4	−10.5	−10.6	−10.4	−10.6
Phase (°)	−61	−58.8	−57.8	−62.6	−60.1	−62.3	−63.5
|S16|(dB)	−8.5	−8.8	−8.7	−9.0	−8.7	−8.8	−8.7
Phase (°)	0	0	0	0	0	0	0

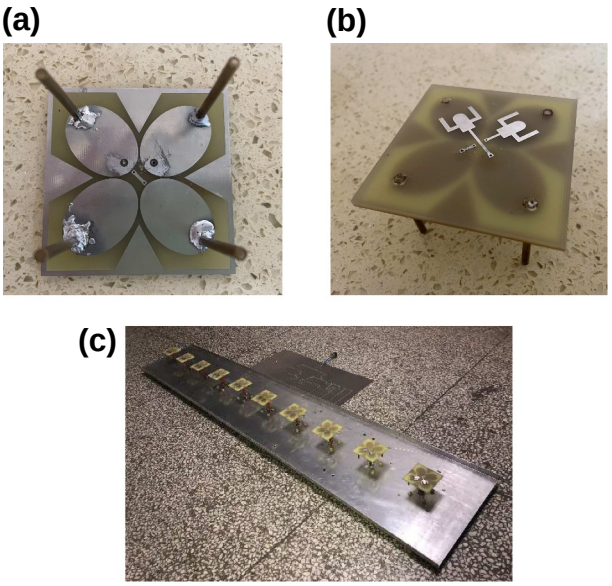

FIGURE 10 Photograph of the fabricated antenna. (a) bottom view of antenna element, (b) top view of antenna element, and (c) antenna array

Measured results validate the design concept and indicate that the proposed array exhibits good radiation characteristics.

ACKNOWLEDGEMENTS

The authors would like to thank Professor Ying Liu from National Key Laboratory of Antennas and Microwave Technology, Xidian University, and Dr. Wei Lin from Global Big Data Technologies Centre, University of Technology Sydney for valuable suggestions. This work was supported by the Fundamental Research Funds for the National Natural Science Foundation of China (Grant no. 61601338 and 61671349) and the Fundamental Research Funds for the Central Universities (No. JB180207).

ORCID

Fanchao Zeng https://orcid.org/0000-0002-1513-1818

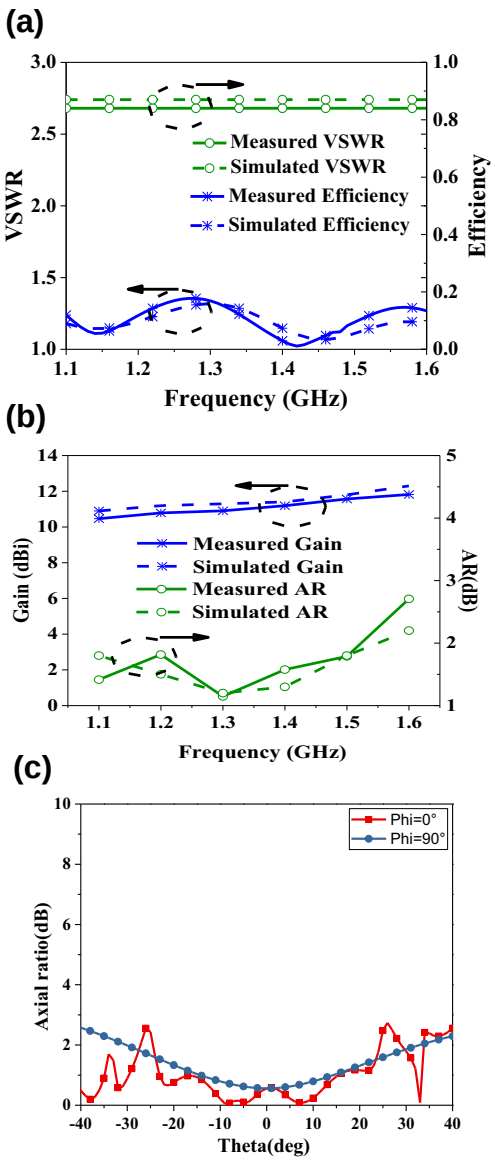

FIGURE 11 Measured and simulated results of (a) VSWR, efficiency, (b) AR, Gain against frequency, and (c) the AR versus angular angle. VSWR, voltage standing wave ratio

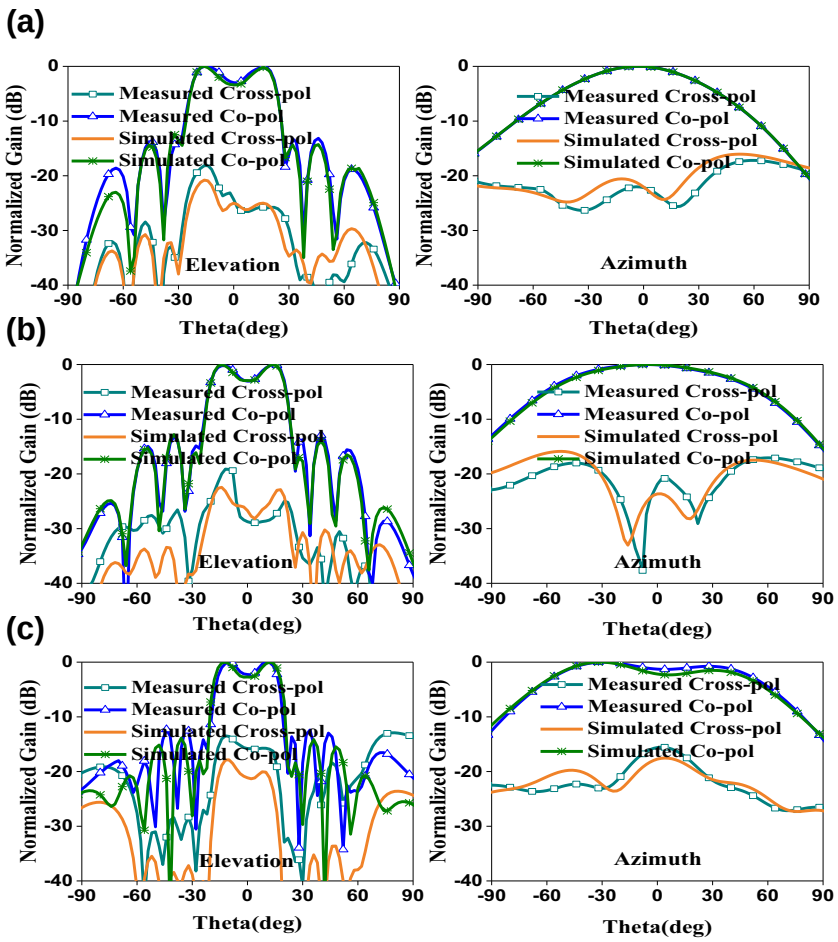

FIGURE 12 Simulated and measured co-polarization polarisation and cross-polarization polarisation patterns at (a) 1.145 GHz, (b) 1.279 GHz, and (c) 1.591 GHz

TABLE 4 Comparison with some recently reported design

Ref.	Antenna type	−10-dB IBW (%,GHz)	Gain (dBic)	3-dB ARBW (%,GHz)
[3]	Dual circular polarisation	8.025–8.4 (4.6%)	6.0	8.025–8.4 (4.6%)
[5]	Bowtie-shaped dipole	2.025–2.125 (4.8%)	About 4	2.025–2.125 (4.8%)
[6]	RHCP Patch antenna	4.12–6 (37.2%)	3.45	4.9–5.2 (5.9%)
[8]	Reflect-array	30	Not given	30
[11]	Patch Antenna	8.0–8.4 (14.9%)	5.5	8.0–8.4 (14.9%)
This Work	Ellipse dipole antenna array	1.1–1.6 (37.0%)	10.2	1.1–1.6 (37.0%)

REFERENCES

1. Gao, S., Luo, Q., Zhu, F.: Circularly Polarized Antennas. Wiley-IEEE Press, Hoboken-Piscataway, USA Nov (2013)
2. EnCheng, W., LuYao, S.: An improved wideband dipole antenna for Global Navigation Satellite system. IEEE Antennas Wirel. Propag. Lett. 13, 1305–1308 (2014)
3. Arnaud, E., et al.: Compact isoflux X-band payload telemetry antenna with simultaneous dual circular polarization for LEO satellite applications. IEEE Antenn. Wirel. Propag. Lett. 99, pp. 1–1 (2020)
4. Long, J., Sievenpiper, D.F.: A compact broadband dual-polarized patch antenna for satellite communication navigation applications. IEEE Antenna. Wirel. Propag. Lett. 14, 273–276 (2015)
5. Choi, E., Lee, J.W., Lee, T.: Modified S-band satellite antenna with isoflux pattern and circularly polarized wide beamwidth. In: IEEE antennas and wireless propagation Letters, 12, pp. 1319–1322 (2013)
6. Ren, X., Liao, S., Xue, Q.: A circularly polarized spaceborne antenna with shaped beam for Earth coverage applications. IEEE Trans. Antenna. Propag. 1–1 (2018)
7. Feng, D., et al.: A broadband low-profile circular-polarized antenna on an AMC reflector. IEEE Antenna. Wirel. Propag. Lett. 16, 2840–2843 (2017)
8. Rodríguez Prado, D., et al.: Design, manufacture, and measurement of a low-cost reflectarray for global Earth coverage. In: IEEE antennas and wireless propagation Letters, vol. 15, pp. 1418–1421 (2016)
9. Wang, W., et al.: Circularly polarized patch antenna with Filtering performance using polarization isolation and dispersive delay line. IEEE Antenna. Wirel. Propag. Lett., 19, 1457–1461 8 (Aug. 2020)
10. Zhang, Z., et al.: Wideband circularly polarized antenna with gain improvement. IEEE Antenna. Wirel. Propag. Lett. 12, 456–459 (2013)
11. Fouany, J., et al.: New concept of Telemetry X-band circularly polarized antenna Payload for CubeSat. IEEE Antenna. Wirel. Propag. Lett, 2987–2991 (2017)

12. Chen, X., et al.: Dual-band circularly polarized antenna using mu-negative transmission lines. IEEE Antenna. Wirel. Propag. Lett., 17, 1190–1194 7 (July 2018)
13. Jeon, K., et al.: X-band isoflux pattern antenna for SAR data transmission. In: 2011 3rd International Asia-Pacific conference on synthetic aperture radar, pp. 1–4. (APSAR), Seoul (2011)
14. Minatti, G., et al.: A circularly-polarized isoflux antenna based on anisotropic metasurface. IEEE Trans. Antenna. Propag. 60(11), 4998–5009 (Nov. 2012)
15. Choi, E., Lee, J.W., Lee, T.: Modified S-band satellite antenna with isoflux pattern and circularly polarized wide beamwidth. IEEE Antenna. Wirel. Propag. Lett. 12, 1319–1322 (2013)
16. Jeong, S., Lee, T., Lee, J.: Optimization for an isoflux pattern from a multiring microstrip array via least-squares regression. IEEE Antenna. Wirel. Propag. Lett. 16, 3005–3008 (2017)
17. Kim, J.H., et al.: Novel waveguide transition structure for isoflux antenna in satellite communication. In: 2012 15 International symposium on antenna technology and applied electromagnetics, pp. 1–4. Toulouse (2012)
18. Fouany, J., et al.: New concept of Telemetry X-band circularly polarized antenna Payload for CubeSat. IEEE Antenna. Wirel. Propag. Lett. 16, 2987–2991 (2017)
19. Gray, D.P., Ravipati, C.B., Shafai, L.: Corporate fed microstrip arrays with non radiating edge fed microstrip patches. In: IEEE Antennas and Propagation Society International Symposium. 1998 Digest. Antennas, vol. 2, pp. 1130–1133. Gateways to the Global Network, Atlanta (1998)

How to cite this article: Zeng F, Zhang ZY, Feng Y, Zuo S, Zhang C, Wang L. Wideband circularly polarised antenna array with isoflux pattern. *IET Microw. Antennas Propag.* 2021;15:1025–1034. https://doi.org/10.1049/mia2.12111